J|A|C|S
ARTICLES
Published on Web 01/05/2005

Decomposition of Triacetone Triperoxide Is an Entropic Explosion

Faina Dubnikova,[†] Ronnie Kosloff,[‡] Joseph Almog,[§] Yehuda Zeiri,*[,‡,⊥] Roland Boese,[||] Harel Itzhaky,[⊗] Aaron Alt,[⊗] and Ehud Keinan*[,⊗,▽,#]

Contribution from the Chemistry Department, Fritz Haber Institute for Molecular Dynamics, and Casali Institute of Applied Chemistry, Hebrew University, Jerusalem 91904, Israel, Chemistry Division, NRCN, P.O. Box 9001, Beer-Sheva 84190, Israel, Fachbereich Chemie der Universitaet Duisburg-Essen, Campus Essen, Universitaetsstrasse 5, 45117 Essen, Germany, Department of Chemistry and Biotechnology, Institute of Catalysis Science and Technology, Technion—Israel Institute of Technology, Technion City, Haifa 32000, Israel, and Department of Molecular Biology and The Skaggs Institute for Chemical Biology, The Scripps Research Institute, 10550 North Torrey Pines Road, La Jolla, California 92037

Received June 14, 2004; E-mail: keinan@tx.technion.ac.il

Abstract: Both X-ray crystallography and electronic structure calculations using the cc-pVDZ basis set at the DFT B3LYP level were employed to study the explosive properties of triacetone triperoxide (TATP) and diacetone diperoxide (DADP). The thermal decomposition pathway of TATP was investigated by a series of calculations that identified transition states, intermediates, and the final products. Counterintuitively, these calculations predict that the explosion of TATP is not a thermochemically highly favored event. It rather involves entropy burst, which is the result of formation of one ozone and three acetone molecules from every molecule of TATP in the solid state.

Introduction

It is commonly accepted that explosive materials, like fuels, are highly energetic compounds that, upon initiation, release their energy content in a fast, exothermic reaction. Accordingly, excessive heat of formation has been considered to be the key property of all explosives.[1] Although this statement is probably correct for most known explosives, particularly those containing nitro groups, including nitroaromatics, nitrate esters, and nitramines, it may not be necessarily the case for less studied families of either conventional or improvised explosives.

Of particular interest in this regard is the group of peroxide-based explosives, including triacetone triperoxide (TATP, **1**), diacetone diperoxide (DADP, **2**), and hexamethylene triperoxide diamine (HMTD, **3**) and their analogues (Scheme 1). TATP is one of the most sensitive explosives known, a property that allows its employment as both primary explosive and main charge. With power close to that of TNT (a 10 g sample gave 250 cm^3 expansion in the Trauzl test as compared to 300 cm^3 for TNT),[2] it may be employed for explosive devices. However, due to its low chemical stability and its sensitivity to mechanical stress and open flame, as well as its high volatility (~66% weight loss within 2 weeks at room temperature), **1** has not been extensively used.[3,4]

Scheme 1

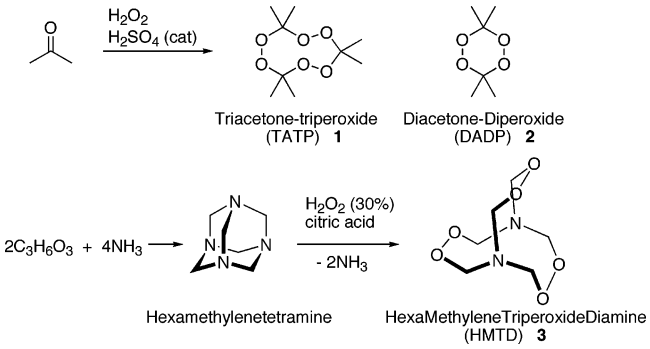

Unlike most conventional explosive devices, those made of **1** contain neither nitro groups nor metallic elements, making its detection by standard methods quite difficult. Furthermore, **1**, which has a quite unsuspicious appearance, reminiscent of white sugar, has no significant UV−vis or fluorescence spectra.

[†] Chemistry Department, Hebrew University.
[‡] Fritz Haber Institute for Molecular Dynamics, Hebrew University.
[§] Casali Institute of Applied Chemistry, Hebrew University.
[⊥] Chemistry Division, NRCN.
[||] Universitaet Duisburg-Essen.
[⊗] Technion−Israel Institute of Technology.
[▽] The Scripps Research Institute.
[#] Incumbent of the Benno Gitter & Ilana Ben-Ami Chair of Biotechnology, Technion.

(1) (a) Politzer, P.; Murray, J. S.; Jorge M.; Seminario, J. M.; Lane, P.; Grice, M. E.; Concha, M. C. *J. Mol. Struct. (THEOCHEM)* **2001**, *573*, 1−10. (b) Iyer, S.; Slagg, S. In *Structure and Reactivity*; Liebman, J. F., Greenberg, A., Eds.; VCH Publishers: New York, 1988; Chapter 7. (c) Kohler, J.; Meyer, R. *Explosives*, 4th ed.; VCH Publishers: New York, 1993. (d) Politzer, P.; Murray, J. S.; Grice, M. E.; Sjoberg, P. In *Chemistry of Energetic Materials*; Olah, G. A., Squire, D. R., Eds.; Academic Press: New York, 1991; Chapter 4. (e) Kamlet, M. J.; Jacobs, S. J. *J. Chem. Phys.* **1968**, *48*, 23−35.
(2) Meyer, R. *Explosives*; Verlag Chemie: Weinheim, New York, 1977.
(3) Commission on Physical Science, Mathematics and Applications. *Containing the threat from illegal bombings: An integrated national strategy for marking, tagging, rendering inert and licensing explosives and their precursors*; National Academy Press: Washington, DC, 1998.

10.1021/ja0464903 CCC: $30.25

Its detection has therefore been limited to IR/Raman spectroscopy and mass spectrometry coupled with chromatographic methods.[5] We have developed a sensitive kit for identification of **1** and other peroxide explosives that is based on enzyme-catalyzed oxidation of organic substrates by hydrogen peroxide to produce colored pigments.[6] Other groups have also used either similar enzymatic techniques[7] or uncatalyzed oxidation reactions.[8]

While studying the properties of **1** and **2**, we discovered large proportions of acetone in their post-blast residues.[9] Other studies on the thermal decomposition of alkyl cyclic peroxides have also reported that the main product was the parent ketone and not oxidation products. This was the case, for example, with tricyclohexylidene triperoxide,[10] tributanone triperoxide,[11] **1** in acetone solution,[12] **1** in toluene solution,[13] and **1** in the gas phase,[13] as well as **2** in benzene solution[14] and in the gas phase.[15] These observations led us to suspect that large negative enthalpy of decomposition may not be the origin of the explosive properties of these materials.

Here we report, on the basis of a computational study of the thermal decomposition pathways of **1**, that the explosion of this compound is not a thermochemically highly favored event. It rather involves entropy burst, which is the result of the formation of four gaseous compounds from one molecule of **1** in the solid state. Thus, the three isopropylidene units and the six oxygen atoms in the molecule do not play the roles of fuel and oxidant, respectively. Contrary to what is expected, the isopropylidene units play merely the role of a molecular scaffold that holds the three peroxide units in close spatial proximity and appropriate orientation for a chain reaction. This structural organization of **1** allows for an efficient cascade of mechanistic events, initiated by the homolytic cleavage of one peroxide bond with consecutive cleavage of the adjacent C−O and O−O bonds in the same molecule, followed by initiation of neighboring molecules in the condensed phase. The method of calculation, which employed the cc-pVDZ basis set at the DFT B3LYP level, was also used for obtaining the ground-state structure and vibrational IR and Raman spectra of **1**. The good agreement between the calculated and experimental data testifies for the reliability of this theoretical approach.

Results and Discussion

Methods of Calculation. The objective of the calculations was to obtain a high degree of accuracy in geometries, binding energies, vibrational frequencies, and transition states. Hence, the calculations were carried out using the density functional theory (DFT)-based method as implemented in the Gaussian 98 code package with an appropriate basis set.[16] This approach is based on the three-parameter hybrid density functional method with the Lee−Yang−Parr correlation functional approximation (B3LYP).[17,18] The Dunning correlation-consistent polarized valence double-ξ (cc-pVDZ) basis set[19] was employed. The structures that had diradical character were located using the unrestricted uB3LYP method wave function with the destructive $\alpha-\beta$ and spatial symmetry. This spin-unrestricted approach has been demonstrated to describe correctly diradical intermediates as well as transition states when multireference problems are present.[20] The uB3LYP method yields good and reliable results, yet economic in terms of required computer time, for rather large molecular systems.

Structure optimization of the reactants and products as well as some transition states was performed by the Berny geometry optimization algorithm[21] without any symmetry constrains. To identify more accurately the transition state in complicated cases, the relaxed potential energy surface scan and the combined synchronous transit-guided quasi-Newton (STQN) method[22] was employed. The vibrational analysis of the structures was performed at the same level of theory in order to characterize reliably the optimized structures as local minima or as transition states. All the calculated frequencies, the zero-point energies, and the thermal energies correspond to harmonic oscillators. The calculations of intrinsic reaction coordinates (IRCs) using internal coordinates were performed in order to examine whether the transition states under consideration connect the expected reactants and products. These calculations were performed for all the transition states at the B3LYP level of theory. The basis set used was the same as that used for the stationary point optimizations.

Adducts, consisting of two or more species, along the decomposition pathways were identified as local minima on the

(4) (a) Muller, D.; Abramovich-Bar, S.; Shelef, R.; Tamiri, T.; Sonenfeld, D.; Levy, A. The post-explosion analysis of TATP; Presented at the 4th Conference of the Israel Society of Analytical Chemists, Tel-Aviv, Israel, January 24−25, 2001. (b) Zitrin, S.; Kraus, S.; Glattstein, B. Identification of two rare explosives. *Proceedings of the International Symposium on the Analysis and Detection of Explosives*, Quantico, VA, March 29−31, 1983; FBI, U.S. Department of Justice: Washington, DC, 1984; pp 137−141. (c) Chladek, J. The identification of organic peroxides. In *Advances in the Analysis and Detection of Explosives*, Proceedings of the 4th International Symposium on the Analysis and Detection of Explosives; Yinon, J., Ed.; Kluwer Academic Publishers: Dordrecht, The Netherlands, 1993; pp 73−76. (d) White, G. M. *J. Forensic Sci.* **1992**, *37*, 652−656. (e) Evans, H. K.; Tulleners, F. A. J.; Sanchez, B. L.; Rassmusen, C. A. *J. Forensic Sci.* **1986**, *31*, 1119−1125.

(5) Widmer, L.; Watson, S.; Schlatter, K.; Crowson, A. *Analyst* **2002**, *127*, 1627−1632.

(6) Keinan, E.; Itzhaky, H. Method and kit for peroxidase detection of peroxide-type concealed explosives. PCT Int. Appl. WO 9943846 A1, Sept 2, 1999; *Chem. Abstr.* **1999**, *131*, 172322; AN 566211, 1999; U.S. Pat. Appl. 09/914,268, 1999.

(7) (a) Schulte-Ladbeck, R.; Kolla, P.; Karst, U. *Analyst* **2002**, *127*, 1152−1154. (b) Schulte-Ladbeck, R.; Karst, U. *Anal. Chim. Acta* **2003**, *482*, 183−188. (c) Schulte-Ladbeck, R.; Kolla, P.; Karst, U. *Anal. Chem.* **2003**, *75*, 731−735.

(8) Bellamy, A. J. *J. Forensic Sci.* **1999**, *44*, 603−608.

(9) Eitan, I.; Keinan, E.; Itzhaky, H.; Sadwin, L. TATP, HMTD and peroxide-based IEDs. Detection, characterization, determination of explosive properties and neutralization; Confidential report, Israel, October 1998.

(10) Sanderson, J. R.; Story, P. R. *J. Org. Chem.* **1974**, *39*, 3463.

(11) Eyler, G. N.; Canizo, A. I.; Alvarez, E. E.; Cafferata, L. F. R. *An. Asoc. Quim. Argent.* **1994**, *82*, 175−181.

(12) Mateo, C. M.; Eyler, G. N.; Alvarez, E. E.; Canizo, A. I. *Inf. Tecnol.* **1998**, *9*, 19.

(13) (a) Eyler, G. N.; Mateo, C. M.; Alvarez, E. E.; Canizo, A. I. *J. Org. Chem.* **2000**, *65*, 2319−2321. (b) Oxley, J. C.; Smith, J. L.; Chen, H. *Propellants, Explos., Pyrotech.* **2002**, *27*, 209−216.

(14) Cafferata, L. F. R.; Eyler, G. N.; Mirifico, M. V. *J. Org. Chem.* **1984**, *49*, 2107−2111.

(15) Cafferata, L. F. R.; Lombardo, J. D. *Int. J. Chem. Kinet.* **1994**, *26*, 503−509.

(16) Frisch, M. J.; Trucks, G. W.; Schlegel, H. B.; Scuseria, G. E.; Robb, M. A.; Cheeseman, J. R.; Zakrzewski, V. G.; Montgomery, J. A., Jr.; Stratmann, R. E.; Burant, J. C.; Dapprich, S.; Millam, J. M.; Daniels, A. D.; Kudin, K. N.; Strain, M. C.; Farkas, O.; Tomassi, J.; Barone, V.; Cossi, M.; Cammi, R.; Mennucci, B.; Pomelli, C.; Adamo, C.; Clifford, S.; Oshterski, J.; Petersson, G. A.; Ayala, P. Y.; Cui, Q.; Morokuma, K.; Malick, D. K.; Rabuck, A. D.; Rahavachari, K.; Foresman, J. B.; Cioslowski, J.; Orviz, J. V.; Baboul, A. G.; Stefanov, B. B.; Liu, G.; Liashenko, A.; Piskorz, P.; Komarini, I..; Gomperts, R.; Martin, R. L.; Fox, D. J.; Keith, T.; Al-Laham, M. A.; Peng, C. Y.; Nanayakkara, A.; Gonzalez, C.; Challacombe, M.; Gill, P. M. W.; Johnson, B.; Chen, M. W.; Wong, M. W.; Andres, J. L.; Head-Gordon, M.; Replogle, E. S.; Pople, J. A. *GAUSSIAN 98*, Revision A.7; Gaussian, Inc.: Pittsburgh, PA, 1998.

(17) Becke, A. D. *J. Chem. Phys.* **1993**, *98*, 5648−5652.

(18) Lee, C.; Yang, W.; Parr, R. G. *Phys. Rev. B* **1988**, *37*, 785−789.

(19) Dunning, T. H., Jr. *J. Chem. Phys.* **1989**, *90*, 1007−1009.

(20) Cremer, D.; Kraka, E.; Szalay, P. G. *Chem. Phys. Lett.* **1998**, *292*, 97−109.

(21) Schlegel, H. B. *J. Comput. Chem.* **1982**, *3*, 214−218.

(22) Peng, C.; Schlegel, H. B. *Isr. J. Chem.* **1993**, *33*, 449−454.

potential energy surface. The energy associated with these weak van der Waals complexes did not include basis set superposition error (BSSE) correction. These complexes are presented only to demonstrate the relative orientation of the different species following decomposition and before separation.

To obtain an estimate of the behavior at the high-pressure limit, first-order rate constants were evaluated using the data obtained in the quantum chemical calculations. The following relation was employed to approximate the rate constant:[23,24]

$$k_\infty = \sigma(kT/h)\exp(\Delta S^{\#}/R)\exp(-\Delta H^{\#}/RT)$$

where h is Planck's constant, k is the Boltzmann factor, σ is the degeneracy of the reaction coordinate, and $\Delta H^{\#}$ and $\Delta S^{\#}$ are the temperature-dependent enthalpy and entropy of the transition state, respectively. Since the decomposition process is a unimolecular reaction, $\Delta H^{\#} = \Delta E^{\#}$, where $\Delta E^{\#}$ is the energy difference between the transition state and the reactant. Here $\Delta E^{\#}$ is defined as $\Delta E^0_{\text{total}} + \Delta E_{\text{thermal}}$, where $\Delta E^0_{\text{total}}$ is the difference between the total energy at the transition state and the energy of the reactant state and $\Delta E_{\text{thermal}}$ is the difference between the thermal energies of these species. The rate to obtain each decomposition intermediate was evaluated using a relation similar to that of k_∞. Each rate constant was evaluated at several temperatures to extract the corresponding Arrhenius parameters from the plot of log k vs $1/T$.

Synthesis and Crystallization of 1 and 2. Since the first reported synthesis of **1** by Wolffenstein in 1895,[25] various protocols for its preparation have been published, some of which are rather unsafe. Interestingly, Wolffenstein himself did not ascribe the explosiveness of **1** to the material itself but rather to traces of ether used for the workup.[25] His uncatalyzed synthesis involved keeping a mixture of acetone (11.6 g) and hydrogen peroxide (50%, 13.6 g) for 4 weeks at room temperature and collecting the resultant precipitate (11.9 g, 26.8%) by filtration followed by recrystallization from ether. The acid-catalyzed synthesis was first described in 1959 by Millas,[26] who slowly added acetone (0.2 mol) at 0 °C to a cold mixture of hydrogen peroxide (50%, 0.2 mol) and sulfuric acid, kept the mixture at 0 °C for 3 h, and then extracted it with pentane. This procedure, which uses large quantities of sulfuric acid, represents a fast route to **1**, but it is rather unsafe, as reported by Oxley.[13b] We found that large quantities of **1** may be prepared safely with minimal amounts of sulfuric acid. For example, acetone (5.6 g, 0.1 mol) was mixed with hydrogen peroxide (30%, 0.1 mol). Concentrated sulfuric acid (5 drops) was added at 0 °C, and the mixture was kept at room temperature for 24 h. The resultant precipitate was collected by filtration with suction and air-dried to afford **1** (4.7 g, 65%) in the form of white crystals. This procedure was scaled up to produce kilogram quantities of **1**. Large single crystals of **1** for X-ray crystallographic studies were obtained by slow sublimation in a closed flask at room temperature.

Compound **1**, which is obtained by precipitation from the above-described reaction between acetone and hydrogen peroxide, is a kinetic product, while **2** is the thermodynamic product. Accordingly, one way to prepare **2** is by acid-catalyzed isomerization of **1** in organic solvents. Thus, dissolving **1** in either chloroform or dichloromethane with a catalytic amount of *p*-toluenesulfonic acid and keeping the solution at room temperature for 1 week afforded pure **2**, which was then collected and recrystallized from hot methanol. An alternative procedure involved slow addition of hydrogen peroxide (30%) to a cold (−5 °C) stirred mixture of acetone and catalytic amounts of methanesulfonic acid in dichloromethane. After the mixture was stirred at −5 °C for an additional 30 min, it was cooled to −20 °C, the organic layer was separated and dried over molecular sieves, the solvent was removed under reduced pressure, and the resultant crude **2** was recrystallized from hot methanol.

Crystal Structure of 2 and 1. The crystal structure of **2** was recently published with cell dimensions similar to those we found, but as a pseudo-merohedral twinned crystal along the reciprocal c^*-axis.[27] Numerous attempts to grow a single crystal of **2** ($C_6H_{12}O_2$, MG = 148.16) from many solvents always resulted in microcrystals which were not suitable for single-crystal X-ray diffraction. However, sublimation in a sealed ampule at room temperature after several weeks and application of very slight temperature gradients led to extremely fine colorless crystals, of which one with the dimensions 0.14 × 0.13 × 0.02 mm^3 could be selected. It was mounted within a nylon wire loop, cooled to −70 °C, and measured on a Bruker SMART CCD system (Mo Kα radiation).

The cell dimensions resulted in a monoclinic metric a = 5.9152(18) Å, b = 5.9221(18) Å, c = 10.585(3) Å, β = 94.344(5)°, V = 369.7(2)Å^3, ρ = 1.331 g cm^{-3}. Due to the poor diffraction power of the small crystal, the data collection was restricted to $2\theta_{\max} = 46.5°$, resulting in 2519 intensities which were merged to 500 observed ($>4\sigma(F_o)$ reflections ($R_{\text{int}} = 0.052$) and used for the crystal structure determination in the space group $P2/c$ (Z = 2), implying molecular C_i symmetry. The anisotropic refinement on F^2 of 49 parameters (Bruker-SHELXTL ver. 6.12) with hydrogen atoms in rigid groups with common isotropic U-values resulted in R_1 = 0.0695 and wR_2 = 0.1741, with a residual electron density of 0.40 e Å^{-3}. A twinning similar to that described in the literature[27] could not be observed due to careful selection of crystals, although some indicators for minor residual twinning remained, such as general F(obs) > F(calc). Any attempts to improve the structure refinement with similar procedures failed, but still, we were able to demonstrate a satisfactory refinement with efforts invested into crystal growths instead of twinning refinement.

The molecular structure (Figure 1) reveals a chair conformation with normal intramolecular distances and angles [O1−C1 1.431(5), O1−O2 1.471(4), O2−C1′ 1.447(5), C1−C3 1.509(8), C1−C2 1.514(6) Å; C1−O1−O2 107.6(3), C1′-O2−O1 107.1(3), O1−C1−C2 113.4(3), O2′−C1−C3 112.6(4), O1−C1−C2 104.4(3), O2′−C1−C2 104.1(4), C3−C1−C2 113.4(3)] and with torsion angles C1−O1−O2−C1′ 65.2(4), O2−O1−C1−O2′ −65.2(4), O2−O1−C1−C3 59.6(4), and O2−O1−C1−C2−175.5(4)°.

The molecular packing consists of slanted stacks of molecules along their crystallographic C_i axis, rotated by 90° (Figure 2). The methyl groups are pointing toward one another with hydrophobic contacts, mutually embedding the central chairs,

(23) Eyring, H. *J. Chem. Phys.* **1935**, *3*, 107−115.
(24) Evans, M. G.; Polanyi, M. *Trans. Faraday Soc.* **1935**, *31*, 875−894.
(25) Wolffenstein, R. *Chem. Ber.* **1895**, *28*, 2265−2269.
(26) Milas, N. A.; Golubovic, A. *J. Am. Chem. Soc.* **1959**, *81*, 6461−6462.
(27) Gelalcha, F. G.; Schulze, B.; Lönnecke, P. *Acta Crystallogr.* **2004**, *C60*, o180−o182.

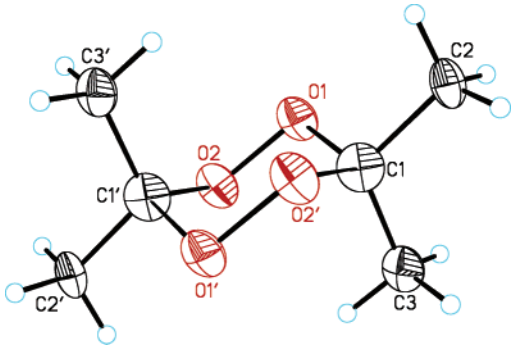

Figure 1. Thermal ellipsoid plot (50%) of **2** with the numbering scheme.

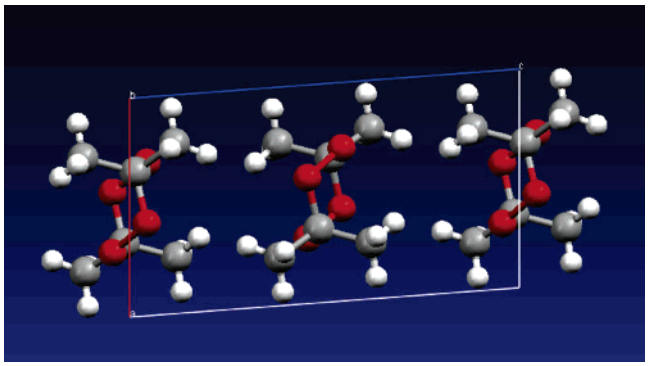

Figure 2. Molecules of **2** in slanted stacks shown in a view down the *b*-axis of the cell.

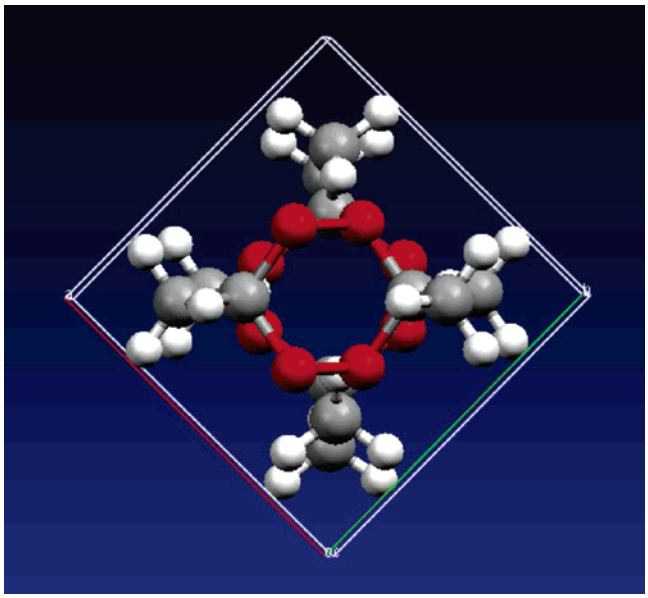

Figure 3. Pseudo-tetragonal packing of **2** apparent with a view down the *c*-axis of the cell.

and thus forming relatively compact packing. The density is 1.331 g cm^{-3}, compared to **1** (vide infra) with 1.272 g cm^{-1}. The pseudo-tetragonal symmetry is revealed not only by the cell dimensions (*a* almost equal to *b*, see Figure 2) but also by the packing diagram (Figure 3), where the tilt of the columns reduces the symmetry to the relatively rare space group *P*2/*c* with $Z = 2$. The projection of the rings is not in an eclipsed staking but following a rotation by about 90°. Intermolecular C—H···O bonds with O···H distances of 2.71 and 2.69 Å produce layers of molecules, in which all oxygen atoms are involved in hydrogen bond bridges (Figure 4). This view reveals

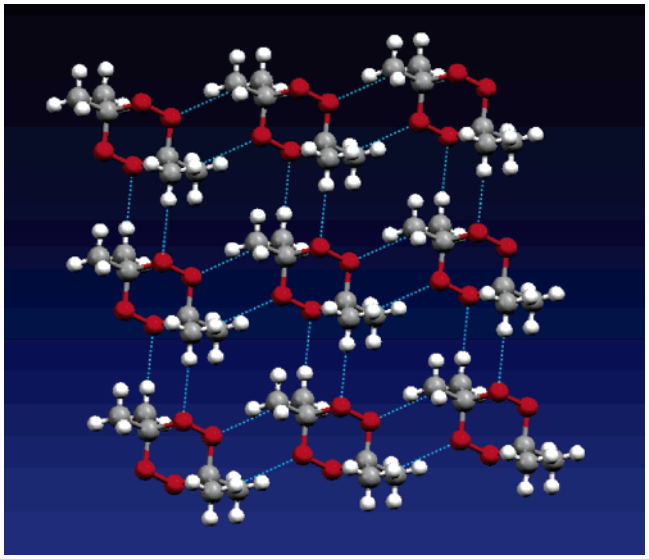

Figure 4. Hydrogen-bonded network via C(sp^3)—H···O bridges in the plane (110).

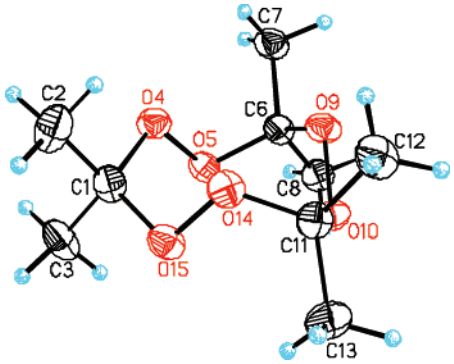

Figure 5. Thermal ellipsoid plot (50%) of the molecule **1** with the numbering scheme.

a networking of columns, each having eight neighboring columns, four closer than the other four, emphasizing the tetragonal motif.

The high volatility of **1** allowed for the formation of larger single crystals by sublimation at atmospheric pressure. We have used this property to obtain the solid-state structure of **1** by X-ray crystallography at low temperatures (all attempts to collect diffraction data at room temperature failed because the crystals disappeared under the X-ray irradiation). The structure was found to be similar to that reported earlier.[28] The crystals are monoclinic with cell parameters $a = 13.788(6)$ Å, $b = 10.664(5)$ Å, $c = 7.894(4)$ Å, $\beta = 91.77(5)°$, $V = 1160.1(9)$ Å^3, with four molecules in the unit cell and space group $P2_1/c$. No solvent molecule is present in the crystal. The molecules have approximately D_3 symmetry, with the nine-membered ring adopting a "twisted boat chair" conformation (Figure 5). The molecular parameters do not indicate any inherent strain, with mean values being C−O 141.9(1), O−O 147.0(2), C−C 1.512(2) Å, O−C−O 112.2(1), C−O−O 107.6(1), C−C−C 113.8(4)°. The crystal packing (Figure 6) consists of stacks around the molecular three-fold axis with no apparent C—H···O interactions, the closest intermolecular contacts being H···H distances of 2.4 Å, which resembles the sum of their van der

(28) Groth, P. *Acta Chem. Scand.* **1969**, *23*, 1311.

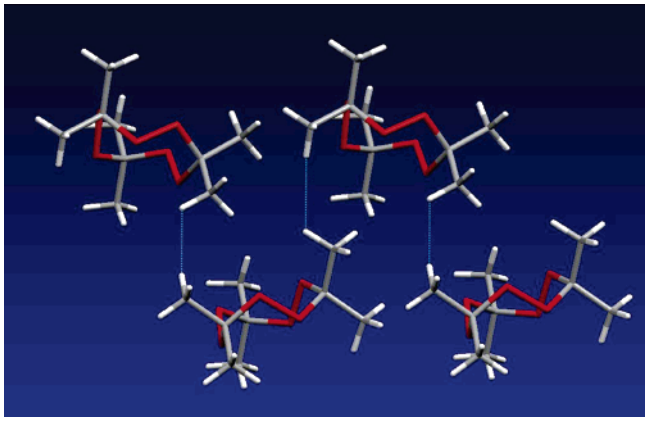

Figure 6. Packing of **1** as capped-stick model along the crystallographic screw axis in a perpendicular view.

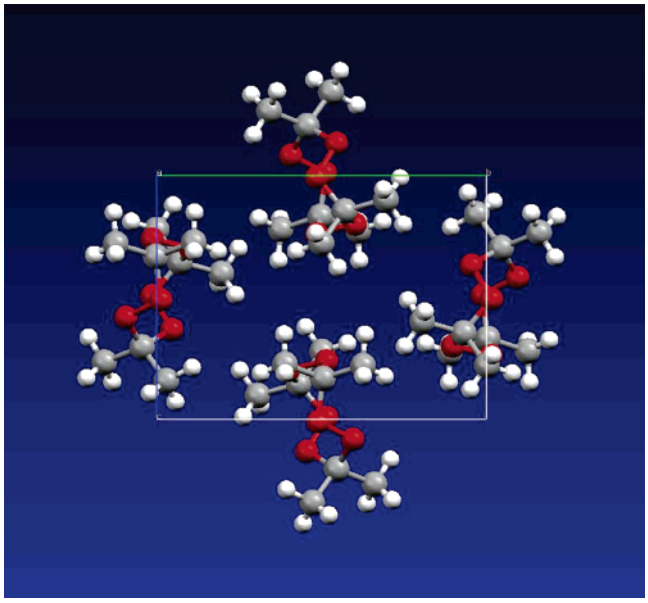

Figure 7. Arrangement of the molecules as ball-and-stick model in a projection down the *a*-axis.

Waals radii. Calculations of lattice energies[29] resulted in −17.35 kcal/mol for **2** and −21.61 kcal/mol for **1**, where the difference does not suggest a significant difference in reactivity. A projection down the *a*-axis (Figure 7) demonstrates the inversion center in the centrosymmetric arrangement in the unit cell. All oxygen atoms are encapsulated by the hydrocarbon environment. The crystal structure is typical of branched hydrocarbons, with hydrophobic space-filling contacts manifesting simple close-packing of hydrophobic molecules. Overall, the structure of **1** differs from that of **2** by the lack of a columnar structure and by the lack of O···H bridges.

One of the reasons for investigating the crystal structures of **1** and **2** was to find explanations for the significant difference between the two compounds as explosive materials, **1** being more potent than **2**. Usually, such differences in the reactivity could result from differences in the inherent molecular strain, the solid-state packing pattern, and packing density. Nevertheless, neither the packing arrangements nor the densities could explain the differences. The lack of CH···O hydrogen bonds in

(29) Cerius2, SGI Version, Dreiding force field with optimization of the molecular geometries and constraints on translation, rotation and the cell parameters according to the experimental values.

Table 1. Comparison between the Calculated and Measured Bond Lengths (Å) and Bond Angles (deg) of **1** and **2**

	TATP, **1**		DADP, **2**	
property	expt	calc	expt	calc
O−C	1.419, 1.418, 1.417	1.422	1.433	1.433
O−C	1.422, 1.421		1.442	
O−O	1.466, 1.471, 1.473	1.458	1.458	1.458
C−C	1.512, 1.514, 1.516	1.528	1.505	1.522
C−C	1.505, 1.510	1.529	1.518	1.524
O−C−O	112.2, 112.5, 112.8	112.9	107.0	108.1
O−C−C	102.7, 103.2, 107.8	102.9	104.4, 104.6	104.6
O−C−C	112.1, 112.5, 112.8	112.3	112.9, 113.4	112.5
O−O−C	107.6, 112.8	108.6	107.3	108.0
C−C−C	113.0, 114.2	113.6	113.9	113.8
τ-COOC		133.9		63.3

1 and the pseudo-tetragonal arrangement of **2** provide no obvious rationale for the differences in reactivity.

Calculations of the Molecular Ground-State and Spectral Properties. The accuracy of the method was established by calculating the ground-state properties of **1** and **2**. The geometries obtained were compared to the above-described X-ray crystallographic data. The good agreement between the calculated and experimental results (Table 1) is noteworthy, considering the fact that the calculation was performed on an isolated molecule in the gas phase, while the experimental data correspond to the solid-state structure. This agreement suggests that the intermolecular forces in the solid phase are too weak to cause any significant alteration of the molecular geometry.

Recently, Buttigieg et al.[30] recorded the IR and Raman spectra of **1** in solution (dissolved in toluene which was allowed to evaporate). We have calculated the frequencies associated with the ground electronic potential energy surface of **1**. The results, frequencies, and intensities obtained from the calculations are superimposed on the experimental data (Figures 8 and 9). The

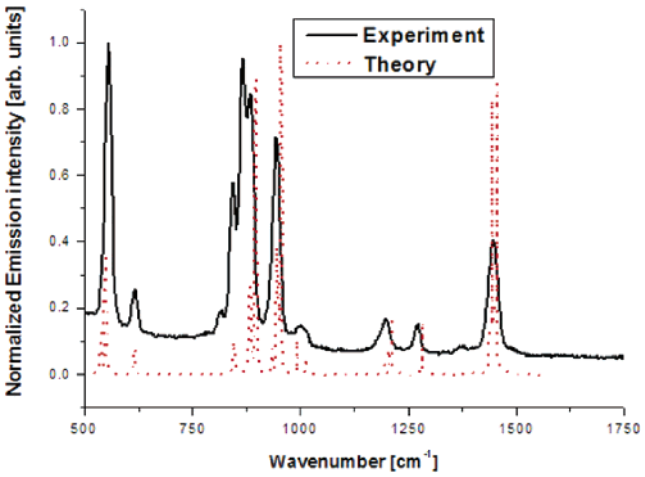

Figure 8. Calculated Raman lines of **1** superimposed on the experimental spectrum.[22]

calculations confirm the published assignment of the bands near 1420 (1470 in the experiment) and 1390 (1370 in the experiment) cm^{-1} as associated with the methyl group motion. The bands near 1200 cm^{-1} are related to the C−O stretch, while the group of bands between 850 and 1000 cm^{-1} are assigned to the peroxide O−O stretch. The low-frequency bands near

(30) Buttigieg, G. A.; Knight, A. K.; Denson, S.; Pommier, C.; Denton, M. B. *Forensic Sci. Int.* **2003**, *135*, 53059.

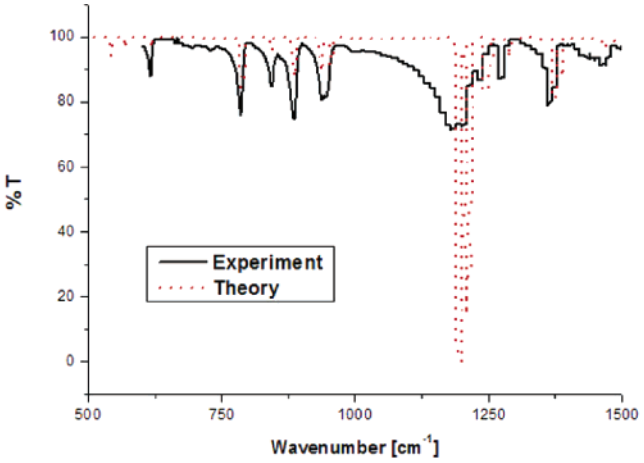

Figure 9. Calculated IR lines of **1** superimposed on the experimental spectrum.[22]

550−600 cm^{-1} are associated, according to the calculations, with the O−C−O bending motion.

TATP Decomposition Mechanism. In our previous work, electronic structure calculations were used to study the Lewis-acid-promoted decomposition of **1**.[31] The Lewis-acidic metal ions studied included Li^+, Cu^+, Zn^{2+}, Cd^{2+}, In^{3+}, Sb^{3+}, Sc^{3+}, and Ti^{4+}. The calculations yielded a detailed picture of the structure and conformation of the free molecule **1** and its complexes with the metal ion. Among all of the metal ions studied, the largest binding energy was found between **1** and In^{3+}. Furthermore, these calculations predicted that the complexation of either Sb^{3+} or Ti^{4+} to **1** would result in ring opening by heterolytic cleavage of a C−O bond, in analogy to the known Lewis-acid-catalyzed cleavage of ketals, to finally produce three molecules of dimethyldioxirane, which were still coordinated to the metal cation.

The low bond energy of the O−O bond renders peroxide-containing molecules, including **1**, heat and shock sensitive. It is expected that the thermal decomposition of these compounds would be initiated by homolytic dissociation of the peroxide bond. Intuitively, it is expected that the peroxide-based explosives would liberate much energy upon decomposition and their energy content would depend on their carbon/oxygen ratio. Recent studies, however, revealed that the thermal decomposition of **1** in solution at 151−230 °C is a first-order reaction, exhibiting an Arrhenius dependence on temperature with activation energy of 36.3 kcal/mol and pre-exponential constant of 3.75×10^{13} s^{-1}.[13] The major decomposition products were found to be acetone and carbon dioxide, while the minor products included ethane, methanol, 2-butanone, and methyl acetate. The product ratio was found to depend on the decomposition temperature.[13b]

Table 2. Total Energies E_{total}, Zero-Point Energies, Relative Energies ΔE,[a] Imaginary Frequencies ν,[b] Entropies S,[c] and Spin Contamination $\langle S^2 \rangle$ of All the Species Shown in Figures 10 and 11

species	E_{total} (hartree)	ZPE	S	ν	$\langle S^2 \rangle$	ΔE
1	−804.937751	170.21	125.50		0.0	0.00
TS1	−804.881919	166.50	134.38	(28i)	1.0058	31.33
I	−804.887244	166.66	141.98		1.0061	28.14
TS2	−804.876510	165.82	139.82	(529i)	1.0066	34.04
TS1D	−804.870091	165.45	140.76	(787i)	1.0056	37.70
II	−804.915790	165.86	149.69		0.0	9.43
4 + acetone	−804.932327	167.06	176.59			0.25

[a] Relative energies in kcal/mol. $\Delta E = E_{total}(\mathbf{1}) - E_{total}(i) + \Delta(\mathrm{ZPE})$, where i represents any one of the species in the table. [b] Imaginary frequency in cm^{-1}. [c] Entropies in cal/(K·mol).

As described in the following discussion, our calculations show that the thermal decomposition of **1** is an intricate, multistep process that starts with the dissociation of one of the O−O bonds. The energy diagrams describing the initial stages of the decomposition process include some structural parameters. Additional characteristics of the various intermediates and transition states are given in Table 2. We found that the initial steps could occur via two slightly different pathways. The first

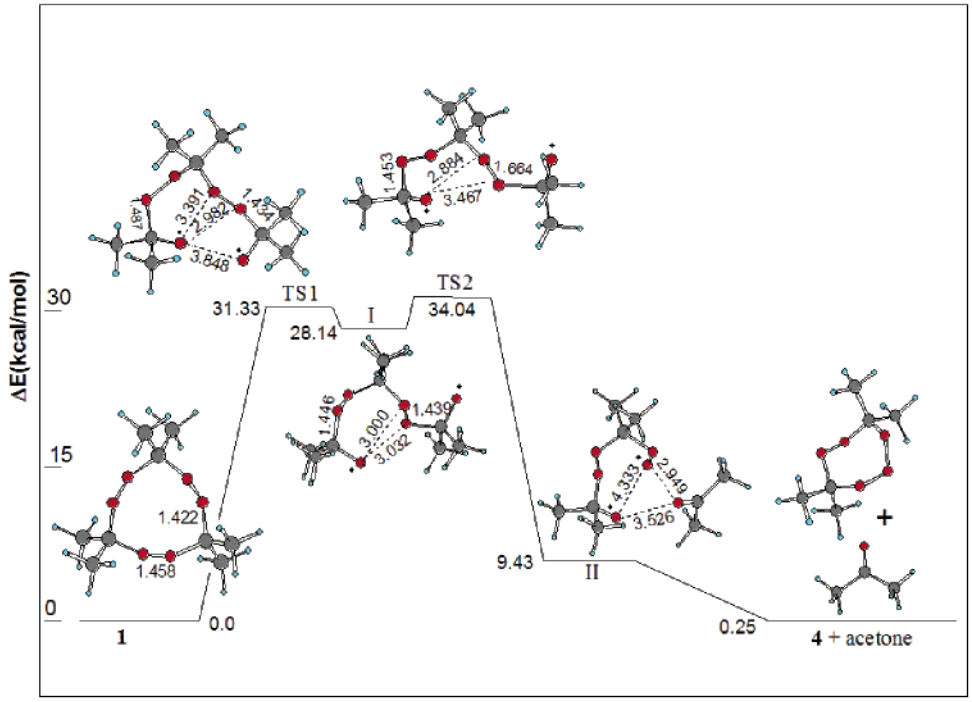

Figure 10.

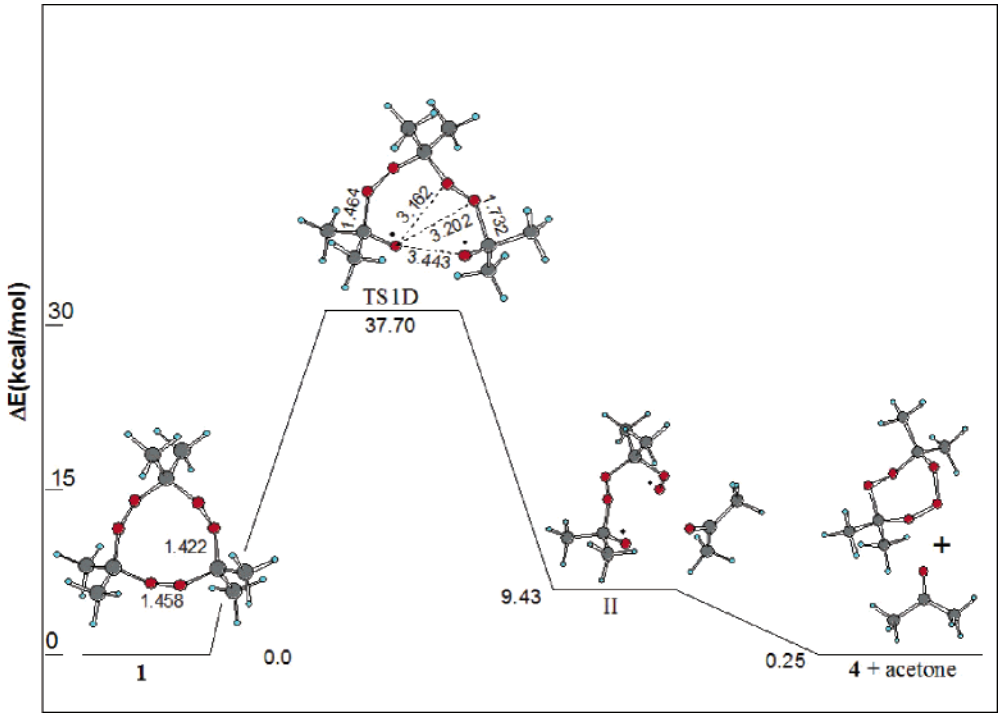

Figure 11.

one consists of the dissociation of one peroxide bond and rotation of the acetone group to yield an intermediate state and a second transition state, associated with the weakening of an adjacent C−O bond (Figure 10). A very similar transition state can be obtained by a single-step mechanism (Figure 11).

Elongation of the O−O bond that leads to transition state **TS1** (Figure 10) is endothermic by approximately 31 kcal/mol. Its dissociation leads to the formation of a diradical intermediate **I**. The imaginary frequency associated with **TS1** is very small (28i cm^{-1}). However, the IRC analysis clearly confirms that **1** and **I** are reactant and product, respectively. The atomic motion related to the normal mode that corresponds to the imaginary frequency of **TS1** indicates that the reaction coordinate consists of rotations of the two $OC(CH_3)_2O$ groups placed on both sides of the dissociating O−O bond. As a result, the distance between the two oxygen atoms of the dissociating peroxide bond is increased in **TS1** to 3.848 Å (compared to 1.458 Å in **1**) and becomes longer than 5 Å in intermediate **I** (Figure 10). In **TS1** the lengths of the two C−O bonds that flank the dissociating O−O bond increase to 1.487 and 1.434 Å, respectively. The lengths of these two C−O bonds change further in **I** to 1.446 and 1.439 Å, respectively. In the second transition state, **TS2**, the length of one of these C−O bonds extends markedly to 1.664 Å (Figure 10). Similar changes are obtained for the geometry of transition state **TS1D**, which is associated with the second pathway (Figure 11). The reaction coordinate in this case is a combination of two normal modes, C−O bond stretching and COO angle bending. The result is a simultaneous breaking of one of the peroxide bonds and one of the nearest neighbors C−O bond (3.443 and 1.732 Å, respectively, in **TS1D**).

Dissociation of the second peroxide bond could be proposed at the next stage of the decomposition process. A corresponding transition state was localized, but the associated energy barrier was found to be too high (∼55 kcal/mol) for this TS to be significant. Consequently, we conclude that the formation of **2** along the thermal decomposition pathway of **1** is not likely to occur. Indeed, formation of **2** was not observed during the decomposition of **1**.[13] A markedly lower decomposition barrier (∼34 kcal/mol) is observed for transition state **TS2** that involves cleavage of a C−O bond following the first peroxide bond dissociation. A slightly higher energy barrier (37.7 kcal/mol) is obtained in the second possible pathway (Figure 11) that involves a very similar transition state, **TS1D**.

Following these two possible transition states, **TS2** and **TS1D**, the reaction coordinate corresponds mainly to a further increase in the bond length of the dissociating C−O bond. The distance between the carbon and the oxygen increases to approximately 3 Å to form an unstable complex, **II** (Figures 10 and 11). It should be noted that the experimental activation energy of approximately 34.8 kcal/mol[13b] is very close to both values of energy barriers obtained in the two possible pathways shown in Figures 10 and 11. Intermediate **II** corresponds to an acetone molecule interacting with a diradical species. Separation of these two species leads to the formation of a free acetone molecule and a seven-membered heterocycle, 4,4,7,7-tetramethyl-1,2,3,5,6-pentoxepane (**4**).

Two alternative decomposition pathways were identified for intermediate **4**. Both pathways, which lead to the formation of a second acetone molecule, are quite complex and involve a number of intermediates and transition states. While describing each decomposition route separately, we use the ground-state energy of **4** as the reference zero energy. Since the energy of acetone together with that of the **4** is equal to that of **1**, the energies along the decomposition pathways actually relate to the ground state of **1**.

Some properties of the various species along the first decomposition pathway are given in Table 3. This pathway begins with simultaneous dissociation of a peroxide bond and

(31) Dubnikova, F.; Kosloff, R.; Zeiri, Y.; Karpas, Z. *J. Phys. Chem. A* **2002**, *106*, 4951−4956.

Table 3. Total Energies E_{total}, Zero-Point Energies, Relative Energies ΔE,[a] Imaginary Frequencies ν,[b] Entropies S,[c] and Spin Contamination $\langle S^2 \rangle$ of All the Species Shown in Figures 12, 13, and 14

species	E_{total}	ZPE	S	ν	$\langle S^2 \rangle$	ΔE
			Figure 12			
4	−611.768023	115.06	102.90		0.0	0.00
TS3	−611.706679	111.56	108.72	(1083i)	0.5934	34.99
III	−611.758415	110.51	129.49		1.0097	1.48
acetone + **IV**	−611.749315	109.58	164.34			6.26
IV	−418.585011	57.58	90.65		1.0022	0.00
			Figure 13			
TS4	−418.564957	56.59	89.49	(615i)	0.8202	11.59
V	−418.597806	57.44	103.03		0.4009	−8.17
acetone + ozone	−418.593270	55.97	132.21			−6.79
			Figure 14			
TS5	−418.582156	56.80	89.61	(363i)	1.1976	1.01
VI	−418.590285	55.76	107.14		2.0131	−5.13
VII (T) + O_2(T)	−418.587669	55.22	126.51			−5.18

[a] Relative energies in kcal/mol. $\Delta E = E_{total}(\mathbf{4}) - E_{total}(i) + \Delta(\text{ZPE})$ or $\Delta E = E_{total}(\mathbf{IV}) - E_{total}(i) + \Delta(\text{ZPE})$, where i represents any one of the species in the table. [b] Imaginary frequency in cm^{-1}. [c] Entropies in cal/(K·mol).

an adjacent C−O bond, leading to the formation of an unstable complex, **III**, via transition state **TS3** (Figure 12). The energy of **III** is only slightly higher than that of **4**. The energy of **TS3** is 35 kcal/mol higher than that of **4**. The reaction coordinate corresponds to the stretching of both O−O and C−O bonds, with bond lengths in **TS3** of 1.917 and 1.885 Å, respectively. Decomposition of **III** results in the formation of a diradical intermediate, **IV**, and an acetone molecule. The combined energy of these products is 6.3 kcal/mol above that of **4**.

The diradical intermediate, **IV**, undergoes further decomposition along two possible pathways. The transition state, **TS4**, of the first pathway (Figure 13) involves C−O bond elongation to 1.755 Å with concomitant bending of the C−O−O angle. The energy of **TS4** is 11.6 kcal/mol above that of **IV** and 18.1 kcal/mol above that of **4**. Once the stretched C−O bond is broken, the energy of the products drops by approximately 7 kcal/mol relative to that of **IV** and a third acetone molecule is formed, together with one molecule of ozone. The combined energy of these decomposition products is approximately 6.8 kcal/mol below that of **IV** and approximately equal to the energy of **1**.

The second decomposition pathway of **IV** (Figure 14) involves a transition state, **TS5**, in which an O−O bond is stretched with a very small (1 kcal/mol) energy barrier, which is 7.5 kcal/mol above the energy of **1**. Further elongation of the O−O bond leads to the formation of an unstable intermediate complex, **VI**, that finally dissociates to give a triplet oxygen molecule and a triplet **VII**. It should be noted that **TS5** has large contributions from excited states that correspond to higher multiplicity. This is demonstrated by its spin contamination value of 1.19 before annihilation and 1.36 after annihilation (Table 3). Thus, this decomposition route is a spin-forbidden path and cannot be correctly estimated by the DFT calculations. This pathway is expected to have low probability due to the long duration associated with such intersystem curve crossings. Further decomposition of the **VII** singlet (vide infra, Figures 16 and 18) yields methyl acetate as the final decomposition product. These last steps correspond to a large energy release. The energy of these final product states is exothermic by approximately 100 kcal/mol relative to **1**. The route described above requires a triplet-to-singlet transition that is exothermic by roughly 2.7 kcal/mol. However, the rate of such a transition between two electronic states that correspond to different spin states is expected to be quite slow, and hence, to have a minor contribution in the decomposition process.

The second decomposition pathway of **4** involves dissociation of an additional O−O bond together with two C−O bonds, leading to the formation of an unstable intermediate complex,

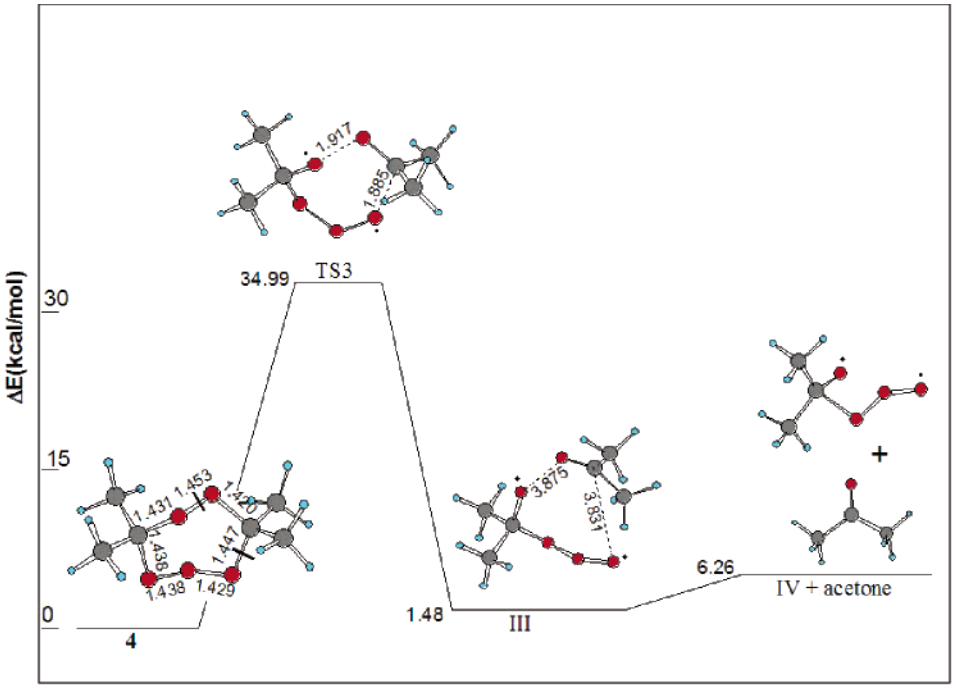

Figure 12.

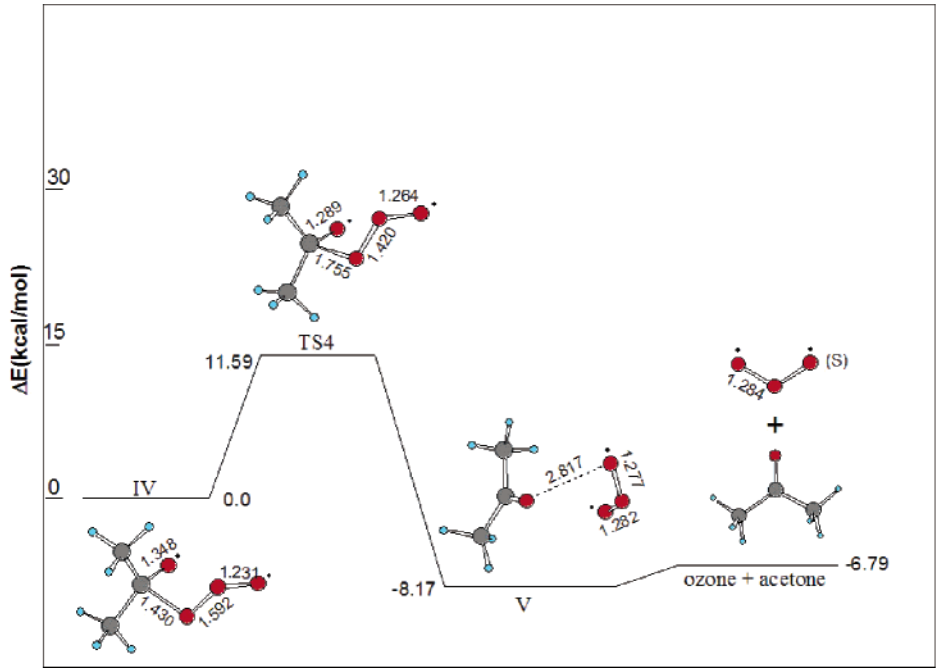

Figure 13.

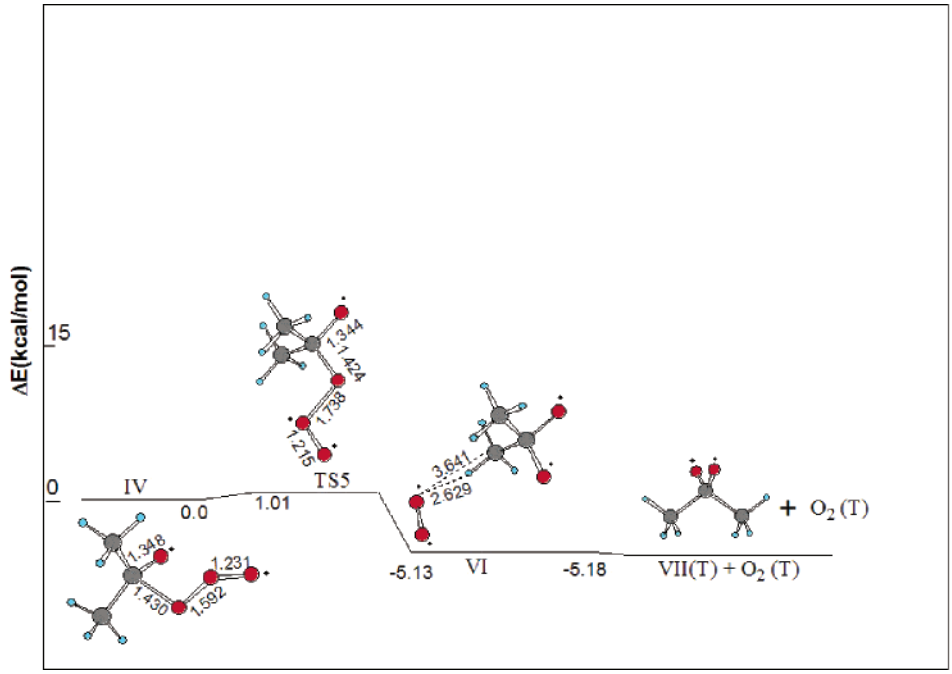

Figure 14.

VIII, via transition state **TS6** with an energy barrier of 28 kcal/mol (Figure 15). The reaction coordinate in this pathway involves simultaneous bending of the O−O−C and C−O−C angles and elongation of one O−O bond and two C−O bonds to 2.247, 2.213, and 1.752 Å respectively, in **TS6**. In **VIII** these distances continue to grow, with corresponding bond lengths of 3.009, 4.057, and 2.988 Å, respectively. **VIII** involves formation of singlet O_2, acetone, and dimethylcarbonyl oxide, **IX**, all at close proximity. After a stable triplet O_2 is formed, the combined energy of these three decomposition products is approximately 5 kcal/mol. The corresponding energy value if a singlet oxygen molecule is formed would be approximately 15 kcal/mol.

The decomposition of **IX** proceeds through transition state **TS7**, with an energy barrier of 22 kcal/mol (∼37 kcal/mol above **1**), leading to the formation of dimethyldioxirane (**5**, Figure 16). The energy of the latter is approximately 3 kcal/mol below the energy of **IX** and 12.9 kcal/mol below that of **1** (Table 4). The reaction coordinate in **TS7** is associated mainly with bending of the O−O−C angle that changes from ∼117° in **IX** to ∼93° in **TS7** and further to ∼65° in **5**.

Compound **5** can undergo a hemolytic ring-opening process via transition state **TS8** to produce the **VII** intermediate, which is thermodynamically less stable than **5** by nearly 13 kcal/mol. This value stands in good agreement with the values obtained for the energy difference between **5** and **VII**, calculated using

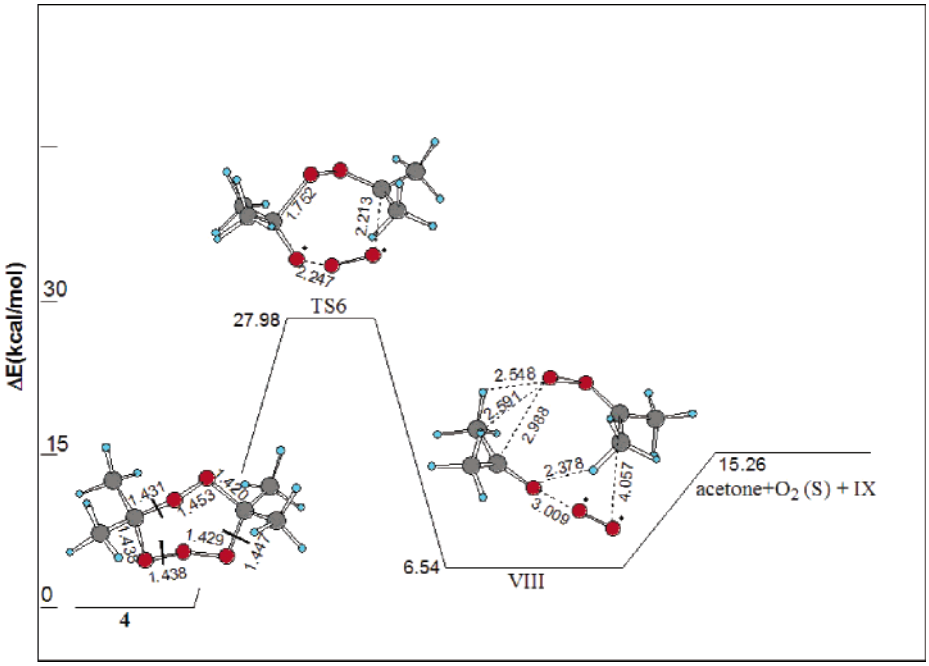

Figure 15.

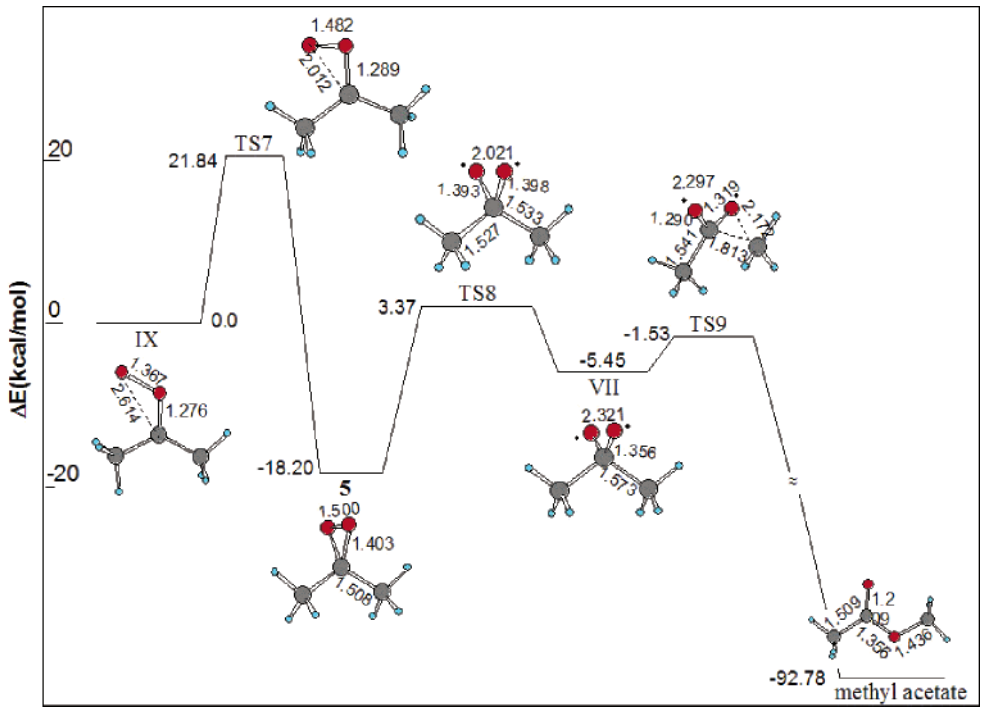

Figure 16.

CCSD(T), MR-AQCC, and B3LYP methods with different triple-ξ basis sets.[20] The energy barrier of this step is 21.57 kcal/mol relative to **5**, again in good agreement with the value of 23 kcal/mol reported earlier.[20] Intermediate **VII** undergoes unimolecular rearrangement to produce methyl acetate via **TS9**, whose energy is approximately 3 kcal/mol higher than that of **VII**. The process involves bending of the O−C−O angle and further elongation of the O−O bond, from 1.5 Å in **5** to 2.021 Å in **TS8** and 2.321 Å in **VII**. Expectedly, the formation of methyl acetate is exothermic by approximately 93 kcal/mol relative to **IX** and by 80 kcal/mol relative to **1**. The reaction coordinate in this last step of the decomposition process is the combination of two normal modes. The one is the C−C bond stretch and the other is a rotation of one of the C−O bonds relative to the stretched C−C bond. In transition state **TS9**, the C−C bond is practically broken (1.813 Å) but the new C−O bond (2.172 Å) is not yet formed. However, the barrier for this transformation is not large, evidently due to the very large exothermicity associated with this stage.

Another option for decomposition of **5** involves the formation of ethane and carbon dioxide as final reaction products (Figure 17 and Table 4). The transition state for this route, **TS10**, is

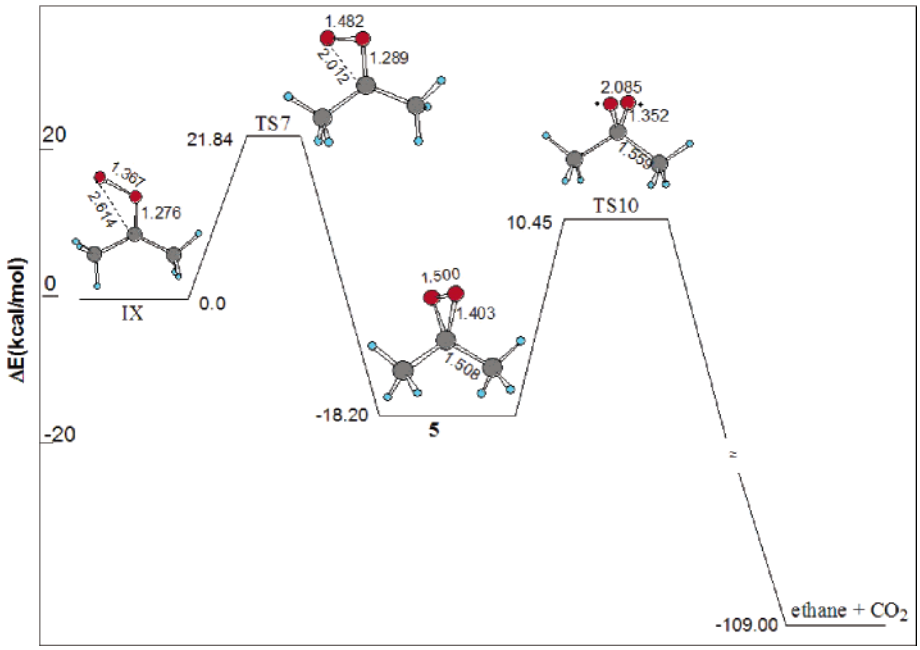

Figure 17.

Table 4. Total Energies E_{total}, Zero-Point Energies, Relative Energies ΔE,[a] Imaginary Frequencies ν,[b] Entropies S,[c] and Spin Contamination $\langle S^2 \rangle$ of All the Species Shown in Figures 15−17

species	E_{total}	ZPE	S	ν	$\langle S^2 \rangle$	ΔE[a]
			Figure 15			
4	−611.768023	115.06	102.90		0.0	0.00
TS6	−611.717580	111.39	112.28	(399i)	0.9145	27.98
VIII	−611.749890	110.22	141.09		1.0027	6.54
acetone + O_2 + **IX**	−611.733569	108.71	195.45			15.52
IX	−268.251637	54.36	74.95		0	0.00
			Figure 16			
TS7	−268.215245	53.37	73.33	(459i)	0	21.84
5	−268.281406	54.84	73.51		0	−18.20
TS8	−268.243747	52.78	73.72	(946i)	0.8447	3.37
VII	−268.257878	52.83	76.02		0.9163	−5.45
TS9	−268.252149	52.51	75.02	(499i)	0.5011	−2.17
methyl acetate	−268.401806	55.81	77.88			−92.78
			Figure 17			
TS10	−268.232286	52.66	73.30	(397i)	0.9888	10.45
ethane + CO_2	−268.427760	52.84	102.33			−109.00

[a] Relative energies in kcal/mol. $\Delta E = E_{total}(\mathbf{4}) - E_{total}(i) + \Delta(\text{ZPE})$ or $\Delta E = E_{total}(\mathbf{IX}) - E_{total}(i) + \Delta(\text{ZPE})$, where i represents any one of the species in the table. [b] Imaginary frequency in cm^{-1}. [c] Entropies in cal/(K·mol).

associated with a relatively high energy barrier 18.9 kcal/mol above the energy of **1** and ∼28.7 kcal/mol above that of **5**. Although the activation energy of **TS10** is much larger than that of **TS9**, the exothermicity of this step is also higher, ∼109 kcal/mol, as compared with ∼93 kcal/mol for the formation of methyl acetate. The reaction coordinate in this case involves bending of the C−O−C angle together with the C−C bond stretch. In the transition state, the length of both C−O bonds decreases to 1.352 Å from a value of 1.403 Å in **5**. This value decreases further to 1.168 Å upon formation of the CO_2 product. The two methyl radicals that are produced during formation of CO_2 combine to yield ethane.

Compound **5** is a known oxidant[20] that has been extensively used in organic synthesis for epoxidation and other oxygenation reactions, including reactions that involve oxygen insertion into an unactivated alkane C−H bond.[32,33] Hence, the formation of **5** along the decomposition pathway may induce additional reactions, including oxygenation of either **1** or various decomposition intermediates and products. For example, **5** can react with ethane to produce acetone and ethanol. Such a reaction is expected to be exothermic by ∼70 kcal/mol and to proceed along a pathway with a relatively low energy barrier of up to ∼30 kcal/mol.

Overall Decomposition Pathway. Scheme 2 shows the complete map of all possible decomposition pathways of **1**, and Figure 18 shows the energy values of all transition states and intermediates of the calculated thermal decomposition, including the $\Delta H^{\circ}_{reaction}$ values for each step and the energy barriers relative to the energy of **1**.

Analysis of the total reaction scheme shows that the initial O−O bond cleavage in **1** is the rate-determining step. The products of this initial step can be obtained via two pathways with slightly different energy barriers and activation enthalpies: ∼34 kcal/mol for the stepwise mechanism (Figure 10) and ∼38 kcal/mol for the concerted pathway (Figure 11). The calculated values of these activation enthalpies and entropies were used to estimate the Arrhenius parameters of the **1** thermal decomposition. The Arrhenius parameters were calculated from the high-pressure limit, as has been discussed above. The rate constant for a concerted mechanism was calculated using the parameters of **1** and **TS1D**. For the stepwise mechanism from **1** to **II**, the rate was calculated using the highest barrier, **TS2**, of the O−O bond cleavage in **1**. More accurate kinetic modeling would lead to an effective barrier slightly larger than the value of **TS2**. Once intermediate **4** is obtained, the rate-limiting step becomes the production of ozone and the third acetone molecule via **TS3**. Accordingly, our calculated Arrhenius parameters

(32) Singh, M.; Murray, R. W. *J. Org. Chem.* **1992**, *57*, 4263−4270.
(33) Freccero, M.; Gandolfi, R.; Sarzi-Amade, M.; Rastelli, A. *J. Org. Chem.* **2003**, *68*, 811−823.

Scheme 2. Possible Intermediates and Final Products of the Thermal Decomposition of **1**, Including Activation Energy and Reaction Enthalpy for Each Step Relative to **1**

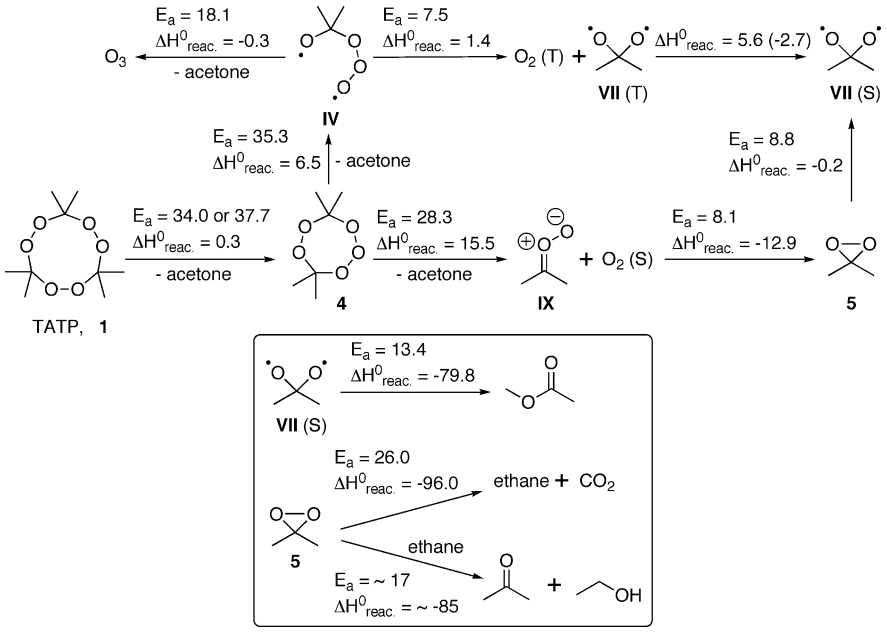

associated with this possibility are

$$k_1 = 5.47 \times 10^{16} \exp(-36.35 \times 10^3/RT)\ \mathrm{s}^{-1}$$

(stepwise mechanism)

$$k_2 = 5.88 \times 10^{16} \exp(-38.82 \times 10^3/RT)\ \mathrm{s}^{-1}$$

(concerted mechanism)

$$k_3 = 5.20 \times 10^{14} \exp(-36.80 \times 10^3/RT)\ \mathrm{s}^{-1}$$

(reaction via **TS3**)

where R is given in units of cal/(K·mol). These rates are comparable with the experimental value:[13b]

$$k = 3.75 \times 10^{13} \exp(-36.09 \times 10^3/RT)\ \mathrm{s}^{-1}$$

(experimental)

For all three possible decomposition rates obtained in the calculations, the pre-exponential values are larger than the one obtained experimentally. However, the activation energies of all three theoretical rates are very close to the experimental value.

Decomposition Kinetics. In order for **1** to sustain an explosive shock wave, the rate of decomposition must match

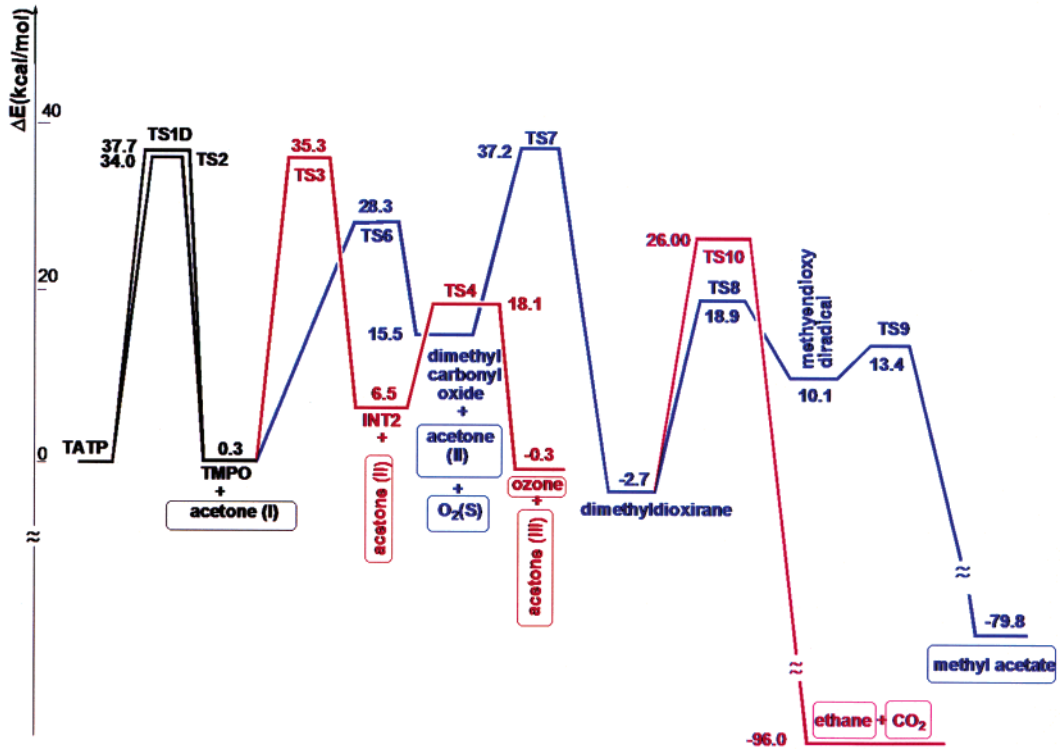

Figure 18.

Table 5. Kinetic Parameters for the Elementary Steps in the Decomposition of **1**

reaction	Arrhenius parameters		rate constant (k, s^{-1})		
	A^a	E_a^b	500 K	650 K	750 K
exptl gas-phase values[13]	3.8×10^{13}	36.1	6.3×10^{-3}	2.8×10^{1}	1.2×10^{3}
1 → **4** + acetone (stepwise mechanism)	5.5×10^{16}	36.4	6.8	3.2×10^{4}	1.4×10^{6}
1 → **4** + acetone (concerted mechanism)	5.9×10^{16}	38.8	6.5×10^{-1}	5.3×10^{3}	2.9×10^{5}
4 → **IV** + acetone	5.2×10^{14}	36.8	4.3×10^{-2}	2.2×10^{2}	9.8×10^{3}
IV → ozone + acetone	1.1×10^{13}	12.2	5.1×10^{7}	8.7×10^{8}	3.1×10^{9}
4 → **IX** + acetone + O_2	6.1×10^{15}	30.4	3.1×10^{2}	3.7×10^{5}	8.5×10^{6}
IX → **5**	8.6×10^{12}	22.3	1.5×10^{3}	2.7×10^{5}	2.7×10^{6}
5 → **VII**	2.8×10^{13}	22.5	4.1×10^{3}	7.6×10^{5}	7.8×10^{6}
VII → methyl acetate	2.2×10^{13}	3.7	5.3×10^{11}	1.3×10^{12}	1.8×10^{12}
5 → ethane + CO_2	2.4×10^{13}	29.6	2.8	2.7×10^{3}	5.7×10^{4}

[a] Pre-exponential factor in s^{-1}. [b] Activation energy in kcal/mol.

the velocity of the detonation wave. Assuming that the shock wave velocity in **1** is approximately 5000 m/s[2] and that the size of a unit cell is in the range of 8−14 Å, the time needed for the shock wave to pass the unit cell is approximately 2×10^{-13} s. Hence, the unimolecular rate of the decomposition should be of the order of 5×10^{12} molecules/s. Considering the Arrhenius relations discussed above, the temperature that corresponds to this rate is roughly 4000 K using k_2 and about 2100 K using k_3 (vide supra). The calculated heat capacity of **1** was found to be $C_v = 173$ and 186 cal/(K·mol) at 2000 and 4000 K, respectively. These decomposition temperatures require heats of 346 and 744 kcal/mol at 2000 and 4000 K, respectively. These values should be compared with the calculated exothermicity of the decomposition process. However, the calculated decomposition exothermicities are far from being sufficient to sustain such high temperatures. As a result, we must conclude that the required heat is obtained by converting volume work[34] to heat in the shock wave. The volume work is obtained by the production of approximately four gas-phase product molecules from the decomposition of a molecule of **1** in the solid state. A rough estimate of the upper limit for the volume work can be obtained by assuming that 1 mol of solid **1** converts to 4 mol of ideal gas products. The approximate pressure increase, assuming an infinitely rapid conversion that occurs in the volume of 1 mol of solid **1**, is of the order of 100 bar. The associated energy content is approximately 2500 kcal/mol. This is the origin of the explosive power of solid **1**.

The exothermicities can be converted to temperatures to yield 650 and 750 K for the methyl acetate and CO_2 decomposition routes, respectively. The rate constants for the various intermediate at these two temperatures are summarized in Table 5. Examination of the rates at both temperatures shows that all rates are too slow in comparison with the shock wave velocity. Thus, to obtain a sustainable explosion, one would need much higher temperatures. As discussed above, such temperatures can be obtained only if volume work, driven by entropy increase, is converted into heat.

Experimental Section

TATP (1). Acetone (5.6 g, 0.1 mol) was mixed with hydrogen peroxide (30%, 0.1 mol), and the mixture was cooled to 0 °C. Concentrated sulfuric acid (5 drops) was slowly added at the same temperature, and the mixture was allowed to reach room temperature and kept at this temperature without stirring for 24 h. The resultant precipitate was collected by filtration with suction and air-dried to afford **1** (4.7 g, 65%) in the form of white crystals. This procedure was scaled up to produce 1−3 kg of **1**. Single crystals for X-ray crystallographic studies were obtained by slow sublimation in a closed flask at room temperature.

Table 6. Crystallographic Data for **1** and **2**

	1	**2**
formula	$C_9H_{18}O_6$	$C_6H_{12}O_4$
formula weight	222.23	148.15
density (g/cm^{-3})	1.272	1.331
T (K)	180(1)	203(2)
crystal size (mm)	0.20 × 0.27 × 0.33	0.14 × 0.13 × 0.02
crystal color	colorless	colorless
crystal system	monoclinic	monoclinic
space group	$P2_1/c$	$P2/c$
a (Å)	13.788(6)	5.9152(18)
b (Å)	10.666(5)	5.9221(18)
c (Å)	7.894(4)	10.585(3)
α (°)	90	90
β (°)	91.77(5)	94.355(5)
γ (°)	90	90
V (Å^3)	1160.1(9)	369.7(2)
Z	4	2
θ_{max} (°)	25.02	23.25
reflns collected	2205	2519
reflns indepen	2055	514
R_{int}	0.0322	0.0522
reflns obsd ($>4\sigma F$)	2055	500
params refined	208	49
R_1 (F)	0.0536	0.0695
wR_2 (F^2, all data)	0.1146	0.1742
residual electron density (e Å^{-3})	0.203	0.40
diffractometer/ radiation	Phillips PW1100/ Mo Kα	Siemens SMART 1K/ Mo Kα

DADP (2). Procedure I. 1 (0.5 g) was dissolved in either dry chloroform or dry dichloromethane, catalytic amounts of *p*-toluenesulfonic acid were added, and the mixture was kept at room temperature for one week. The solvent was removed under reduced pressure, and the residue was recrystallized from hot methanol to yield **2** (0.3 g) in the form of white powder. This convenient procedure is suitable for small quantities of **2**.

Procedure II. A mixture of acetone (62.5 mL, 0.85 mol), methanesulfonic acid (3 mL), and dichloromethane (250 mL) was vigorously stirred at room temperature in a 1 L flask for 10 min and then cooled to −5 °C. Hydrogen peroxide (30% in water, 90 mL, 0.88 mol) was slowly added over a period of 15 min. The mixture was stirred at the same temperature for an additional 30 min and then cooled to −20 °C and transferred to a separatory funnel. The organic layer was collected and dried over molecular sieves (3 Å, 50 g, activated at 150 °C for 24 h) for 10 min and then filtered. Dichloromethane (175 mL) and

(34) Scilly, N. F. *J. Loss Prev. Process Ind.* **1995**, *8*, 265−273.

methanesulfonic acid (35 mL) were stirred in a 2 L flask and then cooled to −5 °C. The above-described dry mixture was added, and the combined mixture was stirred for 40 min. The mixture was then transferred into a separatory funnel and washed three times with ice−water (600 mL). The solvent was removed under reduced pressure to give 24 g of a white powder. This crude product was recrystallized from hot methanol (12 mL of methanol per 1 g of crude **2**) and dried under reduced pressure (2 mmHg) to give pure **2** (20.5 g, 32%). ^{1}H NMR (200 MHz, $CDCl_3$): δ 1.764 (s, 6H), 1.322 (s, 6H). IR: 2956, 1375, 1201, 940, 858, 814, 687 cm^{-1}. DSC: 131.95 °C (140 J/g), 165.25 °C (76 J/g).

Table 6 compares the crystallographic data of **1** and **2**. Additional crystallographic data are available as Supporting Information and from the Cambridge Crystallographic Data Centre.

Conclusions

Both X-ray crystallography and electronic structure calculations were employed to study the explosive properties of **1** and **2**. The structure, vibrational spectrum, and thermal decomposition of **1** were calculated using the cc-pVDZ basis set at the DFT B3LYP level. The applicability of these methods was demonstrated by the excellent agreement between the experimental data and the calculated ground-state structure and vibrational IR and Raman spectra. The calculated thermal decomposition pathway of the molecule **1** was found to be a complicated multistep process with several highly reactive intermediates along the decomposition pathway, including singlet molecular oxygen and various diradicals. Acetone and ozone are predicted to be the main products, along with dioxygen, methyl acetate, ethane, and carbon dioxide. These decomposition products were indeed observed experimentally. The predicted rate-determining step, which has an energy barrier of approximately 34−37 kcal/mol, involves homolytic cleavage of one peroxide bond with concomitant stretching of the neighboring C−O bonds.

It is noteworthy that the calculations predict formation of ozone as well as oxygen molecules in the decomposition process and not the intuitively expected oxidation products. The key conclusion from this study is that the explosion of **1** is not a thermochemically highly favored event. It rather involves entropy burst, which is the result of formation of four gas-phase molecules from every molecule of **1** in the solid state. Quite unexpectedly, the three isopropylidene units of the **1** molecule do not play the role of a fuel that may be oxidized and release thermal energy during the explosion event. Instead, these units function as molecular scaffolds that hold the three peroxide units in close spatial proximity and appropriate orientation for the decomposition chain reaction. It is likely that the detonation of other peroxide-containing materials, including concentrated hydrogen peroxide, is also an entropic explosion rather than an exothermic process.

Acknowledgment. This study was supported by Israel Atomic Energy Commission and the Israel Council for Higher Education. E.K. thanks the Devora and Gensler Foundations for financial support. We thank Moshe Kapon of the Technion for assistance with the crystallographic studies of **1**.

Supporting Information Available: Crystallographic data files of **1** and **2**, in CIF format. This material is available free of charge via the Internet at http://pubs.acs.org. Supplementary crystallographic data for this paper (CCDC 241973 for **1** and 241249 for **2**) can also be obtained free of charge via www.ccdc.cam.ac.uk/conts/retrieving.html (or from the Cambridge Crystallographic Data Centre, 12 Union Rd., Cambridge CB2 1EZ, U.K.; fax +44 1223 336033; e-mail deposit@ccdc.cam.ac.uk).

JA0464903